Su, M., Young, B. and Gardner, L. (2015), "Continuous beams of aluminum alloy tubular cross sections. I: tests and model validation", Journal of Structural Engineering, ASCE, 141(9): 04014232.

CONTINUOUS BEAMS OF ALUMINUM ALLOY TUBULAR CROSS-SECTION - PART I: TESTS AND FE MODEL VALIDATION

by

Mei-Ni Su [1], Ben Young, M.ASCE [2] and Leroy Gardner [3]

ABSTRACT: The aims of this study are to generate experimental data and develop numerical models for aluminum alloy continuous beams, and to utilize the results to underpin the development of revised design methods for indeterminate structures. This paper presents an experimental program and finite element (FE) analyses for two-span continuous beams (i.e. five-point bending) of square and rectangular hollow sections (SHS/RHS). The experimental program comprised 27 five-point bending tests with three different positioning of loads. The testing procedures and key results are reported. The test specimens were manufactured by extrusion, with 18 of grade 6061-T6 and 9 of grade 6063-T5 heat-treated aluminum alloys. The test specimens were non-slender sections, and mostly of Class 1 proportions according to Eurocode 9 (2007). Generally, the specimens failed by the formation of a collapse mechanism comprising three plastic hinges. The distances between the supports and the loading points were varied in order to form the first plastic hinge in different locations, to achieve different load levels between the first hinge and collapse, and to change the rotation demands on the first hinge that formed. The FE models were developed using ABAQUS 6.10-1 (2010), and failure was defined as either when a plastic collapse mechanism was formed or the material fracture strain was reached on the tension flange, whichever occurred first. The numerical models were first validated against the experimentally obtained load-deflection responses, as well as the failure modes. The experimental

and FE ultimate loads were both found to be beyond the theoretical loads corresponding to the formation of the first hinge, as well as the calculated plastic collapse loads. A key characteristic of aluminum alloy, strain hardening, is shown to be particularly significant in both the experimental program and the numerical investigation. The validated FE models are used to generate numerical results through parametric studies in the companion paper. The development of design rules for indeterminate aluminum alloy structural systems is then described.

KEY WORDS: Aluminum alloys; Continuous beams; Experimental investigation; Indeterminate structures; Numerical models; Plastic design; Square and rectangular hollow sections; Testing; Tubular sections.

---

[1] PhD Candidate, Dept. of Civil Engineering, The Univ. of Hong Kong, Pokfulam Road, Hong Kong / Dept. of Civil and Environmental Engineering, Imperial College London, London SW7 2AZ, UK

[2] Professor, Dept. of Civil Engineering, The Univ. of Hong Kong, Pokfulam Road, Hong Kong. E-mail: young@hku.hk

[3] Professor, Dept. of Civil and Environmental Engineering, Imperial College London, London SW7 2AZ, UK. E-mail: leroy.gardner@imperial.ac.uk

INTRODUCTION

Aluminum alloys are non-linear materials, and despite the fact that they are typically less ductile than structural steel and stainless steel, aluminum alloy structural sections may still have sufficient rotation capacity to allow for moment redistribution and to enable the application of plastic design methods (Nethercot et al., 1995). The use of continuity in a structural system brings about several benefits, such as increased load-carrying capacity and reduced deflections. That is to say, for given loads and deflection limits, a more economical cross-section may be used

(Nethercot et al., 1995). Although aluminum alloys have been used in a range of structural engineering applications, underpinned by many international design standards, plastic design methods are not currently applicable in most of these standards. Hence, investigation into the structural response of aluminum alloy indeterminate assemblages is the focus of the present study.

To date, only a limited number of tests have been carried out on continuous beams of nonlinear materials, including those conducted by Panlilio (1947) on two-span systems and those of Welo (1991) on three-span arrangements, with both studies examining aluminum alloy members. More recent experimental studies, exploring the behavior of cold-formed and hot-finished steel and stainless steel elements, have also been performed (Mirambell and Real, 2000; Gardner et al., 2010, 2011; Theofanous et al., 2014). To supplement the limited existing data, a comprehensive laboratory testing program comprising experiments on 27 continuous beams on aluminum alloy square and rectangular hollow sections (SHS/RHS) was conducted at The University of Hong Kong.

In terms of numerical simulations, there have been a number of studies into the structural behavior of determinate aluminum alloy elements, such as plates (Moen et al. 1998; Xiao and Menzemer, 2003), columns (Lai and Nethercot, 1992; Mazzolani et al., 1997; Hassinen, 2000; Zhu and Young, 2006, 2008a, 2008b), and beams under three-point bending (Moen et al., 1999; De Matteis et al., 2001, 2004; Su et al., 2014b) and four-point bending (Opheim, 1996; Wang et al., 2007; Kim and Peköz, 2010; Su et al., 2014b), but simulations of indeterminate aluminum alloy structures are far fewer. Manganiello et al. (2006) developed FE models of indeterminate aluminum alloy structures and validated the models against the five-point bending tests results of Welo (1991). Following validation, the models were used to generate structural performance data for fixed ended beams, continuous beams and portal frames.

The aims of the present study are to examine the behavior of indeterminate aluminum alloy structures through experimentation and numerical modelling, and to use the generated data

to underpin a proposed design method. Two-span continuous beam tests on non-slender, extruded square and rectangular hollow section (SHS/RHS) members are presented. Two material grades (aluminum alloys 6061-T6 and 6063-T5) and three loading configurations are considered. The experimental results are supplemented with additional data established by means of validated finite element models. Finally, comparisons of the results are made with existing design provisions and a newly proposed design method.

EXPERIMENTAL INVESTIGATION

The experimental program comprised 27 continuous beam tests on specimens with a series of different cross-sectional geometries, defined using the symbols illustrated in Fig. 1. The cross-sectional dimensions given in Table 1 are the average measured values for each test specimen in this study. The measured material properties are also provided. The symbols employed in Table 1 are defined as follows: L is the member length, E is the Young's Modulus, f_y is the material yield stress (taken as the 0.2% proof stress), f_u is the material ultimate stress, ε_u is the strain corresponding to the ultimate tensile stress of the material, ε_f is the strain corresponding to the material fracture and n is the exponent of the Ramberg-Osgood expression (Ramberg and Osgood, 1943; Hill, 1944), as given by Equation (1). The stress-strain curves obtained from tensile coupon tests and the Ramberg-Osgood model are compared in Fig. 2. The Webster surface hardness of the material is also reported. These measured cross-sectional dimensions and material properties are used later in this study for both the finite element validation and the calculation of design.

$$\varepsilon = \frac{\sigma}{E} + 0.002\left(\frac{\sigma}{f_y}\right)^n \tag{1}$$

where σ is stress and ε is strain.

The specimens were labeled according to the material strength, cross-sectional dimensions and the test configuration. For example, the label "H55×70×4.2B5I-R" defines an RHS specimen

of high “H” strength aluminum alloy 6061-T6, with cross-sectional dimensions of width B (55 mm) × height H (70 mm) × thickness t (4.2 mm). If the label starts with “N”, it signifies that the specimen is of normal-strength aluminum alloy 6063-T5. The overall nominal length of the continuous beams was 1690 mm for all test specimens. The symbol “B5I” following the dimension refers to the first five-point loading configuration I where L_1=L_2=400 mm, as presented in Fig. 3, while the other two configurations are denoted as B5II where L_2=266.7 mm (i.e. the loads are at one third of the span from the central support) and B5III where L_2=533.3 mm (i.e. the loads are at two thirds of the span from the central support). If a test is repeated, a letter “R” is included in the label. The arrangement of the cross-sectional dimensions also refers to the bending axis. In this case, the specimen H55×70×4.2B5I-R was bent about the major axis, while the specimen H70×55×4.2B5I was bent about the minor axis.

The bending tests were conducted to assess the flexural resistance and rotation capacity of aluminum alloy beams, as well as the significance of strain hardening and moment redistribution. Three symmetrical five-point bending test configurations were employed herein. The loads were applied at two points through a spreader beam, as shown in Figs 3 and 4. Steel rollers and a half round were employed to achieve rotationally free conditions at the beam ends, central support and loading points; longitudinal translation was restrained at the central support. Steel stiffening plates of 100 mm width and 10 mm thickness, as well as wooden blocks inside the tubes were used at the loading points and the mid-span support to prevent web crippling due to load concentration. Furthermore, steel bearing plates were placed between the specimen and rollers/half rounds for the purpose of spreading the concentrated loads. A 1000 kN capacity servo-controlled hydraulic testing machine was used to apply compressive force by displacement control at a constant rate of 0.8 mm/min for all tests. Two 100 mm LVDTs were used to measure the vertical deflection at the loading points. Two 50 mm LVDTs were placed 150 mm either side of the mid-span, in order to

estimate the mid-span rotation. Two 25 mm LVDTs were placed at each end of the beams to measure the end rotation.

The specimens generally failed by material yielding and the formation of a collapse mechanism comprising three plastic hinges (Fig. 5), while some specimens failed due to material fracture on the tension flange (Fig. 6). Inelastic local buckling was also observed for some beams at large deformations. For the loading configurations I and II, the first hinge formed at the central support and the latter two hinges formed at the loading points, while in configuration III the plastic hinges formed in the reverse sequence. In all cases, the ultimate loads attained in the tests were beyond the calculated loads corresponding to the occurrence of the first hinge (F_{h1}), as well as the calculated loads corresponding to the formation of the plastic collapse mechanism (F_{coll}), as presented in Table 2. This is attributed primarily to the significant effect of strain hardening on the cross-section capacity, and is explored further in the companion paper. The load-deflection graphs for all test specimens are given in Fig. 7.

NUMERICAL MODELING APPROACH

The experimental investigation was supplemented by parallel numerical studies. The 27 continuous beam tests described in the previous section were initially replicated numerically by means of the nonlinear finite element (FE) analysis package ABAQUS 6.10-1 (2010). The measured stress–strain curves from the tensile coupon tests conducted on material cut from the flat portions of the test specimens were used in the analyses. The material nonlinearity was included in the FE models by specifying sets of values of true stress and plastic strain to define a piecewise linear response. The relationship between true stress σ_{true} and engineering stress σ, as well as true plastic strain ε_{true}^{pl} and engineering strain ε are given by Equations (2) and (3), respectively.

$$\sigma_{true} = \sigma(1+\varepsilon) \tag{2}$$

$$\varepsilon_{true}^{pl} = \ln(1+\varepsilon) - \sigma_{true} / E \tag{3}$$

The reduced integration four-noded doubly curved shell element S4R was employed in the present study to model the continuous beams. The S4R general purpose shell element has six degrees of freedom per node and provides accurate solutions to problems of the nature addressed in this study (Ellobody and Young, 2005). The steel loading plates utilized in the tests were modeled using 10 mm thick solid elements that were free to rotate in-plane. A uniform mesh size of 10 mm × 10 mm was chosen for all specimens and bearing plates. These element types and size have been shown to perform well for the modeling of aluminum alloy structural members (Zhou and Young, 2008; Zhu and Young, 2006, 2008a, 2008b; Su et al., 2014b).

Residual stresses in the test specimens were not measured and not explicitly modeled in the FE analysis for two reasons: (1) the presence of bending residual stress in extruded aluminum alloy sections is, to a significant extent, implicitly reflected in the material properties obtained from tensile coupon tests (Rasmussen and Hancock, 1993; Jandera et al., 2008); (2) residual stresses have only a very small effect on the load-bearing capacity of aluminum alloy extruded members (Mazzolani, 1994). Initial local geometric imperfections were incorporated in the FE models in the form of the lowest regular elastic buckling mode shape. A linear eigenvalue buckling analysis was therefore initially performed. The initial local geometric imperfection amplitude was defined as 0.2 mm, which represented the average local imperfection amplitudes measured in the test specimens (Su et al., 2014a). It was found that sensitivity of the simulated results to imperfections was generally relatively low.

Even though specimens displayed symmetry in geometry and loading configurations, modeling of the full specimen length (1690 mm) and cross-sections was performed. This was done to ensure that possible anti-symmetric local buckling modes were not suppressed, which, in

some cases, had marginally lower corresponding eigenvalues than their symmetric counterparts (Theofanous et al., 2014). The boundary conditions were modeled in accordance with the tests conducted in the laboratory. Line loads were applied through bearing plates to avoid high load concentrations. Appropriate degrees of freedom were restrained at the bottom flange of the specimens to simulate simple supports. The beams were restrained longitudinally at the mid-span only.

The interfaces between the steel bearing plates and the aluminum alloy specimens were modeled using a contact pair. Hard contact in the normal direction and friction penalty contact (with the friction coefficient = 0.1) in the tangential direction were adopted between the solid plate (master surface) and the beam surface (slave surface). Penetration of the contact pairs was prevented. The loading control employed in the FE analysis was similar to that used in the tests, whereby the load was applied by imposing vertical displacement to the solid bearing plates. The Riks procedure with automatic increment sizing, as described in ABAQUS 6.10-1 (2010), was used to allow the post-ultimate path of the modeled specimen to be captured.

VALIDATION OF NUMERICAL MODEL

In this section, the FE models are validated by the comparison against the 27 physical test results. Comparisons are made in terms of ultimate loads and the corresponding end rotations (Table 2). Failure criteria, failure modes and general load-deformation behavior are also described.

Failure Modes

Observed failure modes included material yielding (Y) with the formation of a plastic collapse mechanism, and tensile material fracture (F). The formation of a collapse mechanism

comprising three plastic hinges was clearly observed in all simulated specimens. Local buckling was also found in the compression flanges of the relatively slender sections when the beam had large deformations. A comparison of the typical failure modes between tested and simulated specimens is depicted in Fig. 8.

In the experimental program, some specimens failed by material fracture at the tension flanges, due to exceedance of the material fracture strain ε_f. This failure mode was accounted for in the FE models by monitoring the tensile strains and identifying when the tensile fracture strain ε_f, as obtained from tensile coupon tests, was reached. This is shown in Fig. 9, where a typical load-deformation response is given. In the graph, the solid dot signifies the point where the strain at the tension flange of the simulated specimen reaches the material fracture strain ε_f, hence signifying tensile failure.

Load-Displacement Behavior

The full load-deflection responses from all tests and simulations were compared; a typical example is shown in Fig. 9. In general, the initial stiffness and the shape of the numerical load-deflection curves closely matched those obtained from the experiments. Overall, good agreement between the experimental and numerical results was observed, though for some cases, the predicted load-bearing capacity deviated to some extent from the test results. On average, ultimate loads F_{FE} were predicted to within 2% of the test results F_{exp} and with a low coefficient of variation (COV = 0.061), as shown in Table 2. The end rotations at ultimate load (θ_{exp} and θ_{FE}) were less accurately captured, but predicted, in most cases within 10% of the experimental measurements, as shown in Table 2. Therefore, it can be concluded that the FE model developed herein is able to simulate accurately the behavior of the tested members and to capture strain hardening and the spread of plasticity in aluminium alloy continuous beams.

Results from the FE models can be used to plot the moment-deflection curves at the plastic hinge locations (i.e. the mid-span support and the loading points), together with the applied load-deflection curve, to assess the load level at which the plastic hinges formed and the degree of moment redistribution. A pair of typical curves for loading configuration II (from specimen H64×64×3.0B5II) is shown in Fig. 10. Key observations from Fig. 10 include: (1) Initially, the moment at the support was approximately twice that in the span, as predicted by elastic bending theory; (2) the support moment therefore reached its ultimate capacity earlier than the span moment, after which the support moment decreased slightly while, at the same time, the span moment kept increasing until reaching its cross-section moment capacity; (3) the applied load continued to increase after the support moment had reached its maximum value, and only dropped when the degree of reduction in the support moment outweighed the increase in the span moment; (4) both the support moment and the span moment achieved capacities greater than the plastic moment M_{pl}, owning to the effect of strain hardening.

CONCLUSIONS

A total of 27 experiments on aluminum alloy square and rectangular hollow section beams, consisting of three different five-point bending configurations, have been presented in this paper. The test specimens were non-slender sections, and were mostly of Class 1 proportions according to Eurocode 9 (2007). Parallel numerical simulations of aluminum alloy continuous beams were performed using ABAQUS 6.10-1 (2010). The results obtained from the developed FE models were compared with those from the tests and it was found that the models were capable of replicating accurately the structural behaviors of the test specimens. The observed failure modes included inelastic local buckling, the formation of a plastic collapse mechanism and tensile facture. A high degree of both strain hardening and moment redistribution was exhibited. The validated numerical models are used to carry out an extensive parametric study in the

companion paper, and thus a database comprising sufficient experimental and numerical results on aluminum alloy continuous beams is formed for the purpose of assessing and developing design rules.

ACKNOWLEGEMENTS

The research work in this paper was supported by a grant from The University of Hong Kong under the seed funding program for basic research. The authors are also grateful to Ms. Mengxi Wu for her assistance in the experimental program as part of her final year undergraduate research project at The University of Hong Kong.

NOTATION

B = Section width

b = Flat width of flange

COV = Coefficient of variation

E = Young's modulus

f_y = Yield strength, taken as the 0.2% proof strength

f_u = Ultimate tensile strength

F_{coll} = Ultimate load level at which the plastic collapse mechanism forms (with cross-sectional capacity at the hinge equal to $W_{pl}f_y$)

F_{FE} = Numerical ultimate load

F_{exp} = Experimental total ultimate load

F_{h1} = Ultimate load level at which the first hinge forms (with cross-sectional capacity at the hinge equal to $W_{pl}f_y$)

H = Section depth

h = Flat depth of web

L = Member length

M_{pl} = $W_{pl}f_y$ is the plastic moment capacity

n = Exponent in Ramberg-Osgood expression

t = Wall thickness

W_{pl} = Plastic section modulus

ε = Engineering strain

ε_f = Material fracture strain

ε_{true}^{pl} = true plastic strain

ε_u = Strain at ultimate tensile stress

θ_{exp} = Rotation at hinge point obtained from tests

θ_{FE} = Rotation at hinge point obtained from FE models

σ = Engineering stress

σ_{true} = True stress

REFERENCES

ABAQUS standard user's manual (version 6.10-1), (2010), Hibbitt, Karlsson and Sorensen, Inc, USA.

De Matteis, G., Landolfo, R., Manganiello, M. and Mazzolani, F.M. (2004) "Inelastic behaviour of I-shaped aluminium beams: numerical analysis and cross-sectional classification", *Computers and Structures* 82 (23-26): 2157–2171

De Matteis, G., Moen, L.A., Langseth, M., Landolfo, R., Hopperstad, O.S. & Mazzolani, F.M. (2001) Cross-Sectional Classification for Aluminium Beams—Parametric Study. *Journal of Structural Engineering, ASCE* 127(3): 271-279.

Ellobody, E. and Young, B. (2005) “Structural performance of cold-formed high strength stainless steel columns”, *Journal of Constructional Steel Research* 61 (12): 1631–1649

European Committee for Standardization (EC9). (2007). “EUROCODE 9: Design of aluminum structures—Part 1-1: General rules—General rules and rules for buildings.” *BS EN 1999-1-1:2007, CEN*.

Gardner, L., Saari, N. and Wang F. (2010) “Comparative experimental study of hot-rolled and cold-formed rectangular hollow sections” *Thin-Walled Structures*, 48 (7): 495–507.

Gardner, L., Wang, F. and Liew, A. (2011). “Influence of strain hardening on the behavior and design of steel structures.” *International Journal of Structural Stability and Dynamics* 11(5): 855-875.

Hassinen, P. (2000). “Compression strength of aluminum columns – Experimental and numerical studies” *c, 241-248, CIMS’2000*, ICP, London, UK

Hill, H.N. (1944). “Determination of stress–strain relations from the offset yield strength values.” *Technical note no. 927.* Washington (DC): National Advisory Committee for Aeronautics.

Jandera, M., Gardner, L. and Machacek, J. (2008) “Residual stresses in cold-rolled stainless steel hollow sections.” *Journal of Constructional Steel Research*, 64(11): 1255-1263

Kim, Y. and Peköz, P. (2010) “Ultimate flexural strength of aluminum sections”, *Thin-walled structures*, 48(10-11): 857-865.

Lai, Y.F.W. and Nethercot, D.A. (1992). “Design of aluminium columns” *Engineering structures* 14(3): 188-194

Manganiello, M., De Matteis, G. and Landolfo, R. (2006) “Inelastic flexural strength of aluminium alloys structures”, *Engineering Structures*, 28(4): 593-608.

Mazzolani, F.M. (1994), *Aluminium alloy structures* 2nd. E&FN Spon Press

Mazzolani, F.M., Piluso, V. and Rizzano, G. (1997) “Numerical simulation of aluminium stocky hollow members under uniform compression” *Proceedings of the 5th international colloquium on Stability and ductility of steel structures*. 1997 July 29-31. Nagoya, Japan

Mirambell, E. and Real, E. (2000) “On the calculation of deflections in structural stainless steel beams: an experimental and numerical investigation” *Journal of Constructional Steel Research*, 54(1): 109-133

Moen, L., Langseth, M., and Hopperstad, O. S. (1998). ‘‘Elastoplastic buckling of anisotropic aluminium plate elements’’ *Journal of Structural Engineering, ASCE*, 124(6):712–719

Moen, L.A., Hopperstad, O.S. and Langseth M. (1999). “Rotational capacity of aluminium beams under moment gradient. I: experiments.” Journal of Structural Engineering, ASCE 125(8), 910-920.

Nethercot, D. A., Li T. Q. and Choo, B. S. (1995) “Required rotations and moment redistribution for composite frames and continuous beams”, *Journal of Constructional Steel Research*, 35(2): 121-163.

Opheim, B. S. (1996). *Bending of thin-walled aluminium extrusions*, PhD Dissertation, Division of Structure Engineering., Norwegian University of Science and Technology

Panlilo, F. (1947). ‘‘The theory of limit design applied to magnesium alloy and aluminum alloy structures.’’ *J. Royal Aeronautical Soc.*, Vol. LI534–571.

Ramberg, W. and Osgood, W. R. (1943) “Description of stress-strain curves by three parameters”, *Technical Note No. 902, National Advisory Committee for Aeronautics*, Washington DC.

Rasmussen, K.J.R. and Hancock, G.J. (1993) “Design of cold-formed stainless steel tubular members. I: Columns.” *Journal of Structural Engineering, ASCE*, 119(8): 23492367.

Su, M., Young, B. and Gardner, L. (2014a) “Testing and design of aluminium alloy cross-sections in compression.” *Journal of Structural Engineering, ASCE*, in press.

Su, M., Young, B. and Gardner, L. (2014b) “Deformation-based design of aluminium alloy beams” *Engineering Structures*, 80, 339-349.

Theofanous, M., Saliba, N., Zhao, O. and Gardner, L. (2014) “Ultimate response of stainless steel continuous beams”. Thin-Walled Structures. 83, 115-127.

Wang, T., Hopperstad, O.S., Lademoa, O.G. and Larsen, P. K. (2007) “Finite element modelling of welded aluminium members subjected to four-point bending”, *Thin-Walled Structures* 45 (2007) 307–320

Welo T. *Inelastic deformation capacity of flexurally-loaded aluminium alloy structures*. Ph.D. thesis. Trondheim (Norway): Division of Structural Engineering, The Norwegian Institute of Technology; 1991.

Xiao, Y. and Menzemer, C. (2003) “Ultimate Compressive Strength of Aluminum Plate Elements”, *Journal of Structural Engineering, ASCE*, 129 (11): 1441-1447

Zhou, F. and Young, B. (2008) “Aluminum tubular sections subjected to web crippling—Part I: Tests and finite element analysis” *Thin-Walled Structures* 46 (4): 339–351

Zhu, J.H. and Young, B. (2006). “Experimental investigation of aluminum alloy thin-walled tubular members in combined compression and bending.” *Journal of Structural Engineering, ASCE* 132(12):1955-1966.

Zhu, J.H. and Young, B. (2008a). “Numerical investigation and design of aluminum alloy circular hollow section columns”, *Thin-Walled Structures* 46 (12): 1437– 1449

Zhu, J.H. and Young, B. (2008b). “Behaviour and design of aluminium alloy structural members”, *Advanced Steel Construction* 4(2): 158-172

Table 1. Measured five-point bending specimen dimensions and material properties obtained from tensile coupon tests

Specimen	B (mm)	H (mm)	t (mm)	L (mm)	E (GPa)	f_y (MPa)	f_u (MPa)	ε_u (%)	ε_f (%)	n	Webster Hardness
H55×70×4.2B5I	54.9	70.0	4.09	1695	70	261	282	5.95	6.45	16	14
H55×70×4.2B5I-R	54.9	69.9	4.08	1649	70	261	282	5.95	6.45	16	14
H70×55×4.2B5I	70.0	54.9	4.10	1702	70	261	282	5.95	6.45	16	14
H50×95×10.5B5I	49.7	94.7	10.34	1646	70	179	220	8.13	14.13	8	13
H95×50×10.5B5I	94.8	49.8	10.38	1696	70	179	220	8.13	14.13	8	13
H64×64×3.0B5I	63.9	63.9	2.86	1693	66	234	248	6.65	9.54	12	12
N50×95×10.5B5I	49.8	94.8	10.38	1696	69	164	211	7.28	13.65	10	11
N70×120×10.5B5I	70.0	119.9	10.42	1690	71	139	194	6.58	14.08	9	11
N120×70×10.5B5I	119.9	69.9	10.27	1652	71	139	194	6.58	14.08	9	11
N120×120×9.0B5I	120.0	120.0	8.89	1700	71	183	225	9.71	14.30	10	11
H55×70×4.2B5II	54.9	69.9	4.09	1652	70	261	282	5.95	6.45	16	14
H55×70×4.2B5II-R	54.9	69.9	4.07	1699	70	261	282	5.95	6.45	16	14
H70×55×4.2B5II	69.9	54.9	4.10	1695	70	261	282	5.95	6.45	16	14
H50×95×10.5B5II	49.7	94.8	10.39	1669	70	192	232	7.17	10.03	13	11
H95×50×10.5B5II	94.7	49.6	10.33	1694	70	179	220	8.13	14.13	8	13
H64×64×3.0B5II	63.9	63.9	2.85	1698	67	232	245	6.82	10.06	12	12
N70×120×10.5B5II	69.9	119.7	10.27	1694	71	139	194	6.58	14.08	9	11
N120×70×10.5B5II	119.8	69.9	10.26	1649	71	139	194	6.58	14.08	9	11
N120×120×9.0B5II	119.9	119.9	8.90	1696	69	188	229	9.10	13.21	11	11
H55×70×4.2B5III	54.9	69.9	4.08	1692	67	207	222	6.77	11.83	16	13
H55×70×4.2B5III-R	54.9	69.9	4.10	1694	70	261	282	5.95	6.45	16	14
H70×55×4.2B5III	69.9	54.9	4.11	1693	65	193	207	5.08	9.84	23	12
H50×95×10.5B5III	49.7	94.8	10.36	1643	70	192	232	7.17	10.03	13	12
H95×50×10.5B5III	94.8	49.7	10.34	1655	70	192	232	7.17	10.03	13	12
H64×64×3.0B5III	63.9	63.9	2.85	1696	66	234	248	6.65	9.54	12	12
N70×120×10.5B5III	69.9	119.8	10.27	1654	71	139	194	6.58	14.08	9	11
N120×70×10.5B5III	119.9	69.9	10.33	1644	71	139	194	6.58	14.08	9	11

Table 2. Comparisons of continuous beam test results with first hinge F_{h1} and plastic collapse F_{coll} loads as well as finite element results

Specimen	*b/t*	Class (EC9)	Failure Mode^	F_{exp} (kN)	θ_{exp} (rad)	F_{exp}/F_{h1}	F_{exp}/F_{coll}	$\frac{F_{\exp}}{F_{FE}}$	$\frac{\theta_{\exp}}{\theta_{FE}}$
H55×70×4.2B5I	11.4	2	Y	114.1	0.072	1.46	1.29	0.99	1.04
H55×70´4.2B5I-R	11.5	2	Y	112.3	0.098	1.40	1.24	0.93	1.01
H70×55×4.2B5I	15.1	2	Y	84.9	0.092	1.29	1.15	1.10	0.91
H50×95×10.5B5I	2.9	1	F	329.9	0.133	1.87	1.67	0.92	0.99
H95×50×10.5B5I	7.1	1	Y	188.2	0.144	1.83	1.63	0.98	0.88
H64×64×3.0B5I	20.4	3	Y	65.3	0.037	1.31	1.17	0.95	0.95
N50×95×10.5B5I	2.9	1	Y	306.7	0.177	1.96	1.74	0.92	1.44
N70×120×10.5B5I	4.7	1	F	532.9	0.121	2.19	1.95	1.05	1.03
N120×70×10.5B5I	9.7	1	Y	362	0.070	2.22	1.97	0.90	0.95
N120×120×9.0B5I	11.5	1	F	655.2	0.102	1.64	1.46	0.99	1.06
H55×70×4.2B5II	11.4	2	F	141.5	0.059	1.74	1.25	1.14	1.16
H55×70×4.2B5II-R	11.5	2	F	130.6	0.060	1.66	1.20	1.05	1.02
H70×55×4.2B5II	15.1	2	Y	120.2	0.056	1.80	1.30	0.96	1.00
H50×95×10.5B5II	2.9	1	F	436	0.111	2.31	1.66	0.92	1.29
H95×50×10.5B5II	7.2	1	Y	222.1	0.111	2.15	1.55	0.92	0.95
H64×64×3.0B5II	20.4	3	Y	80.8	0.026	1.62	1.17	0.94	0.90
N70×120×10.5B5II	4.8	1	F	693.9	0.072	2.87	2.07	1.00	1.33
N120×70×10.5B5II	9.7	1	Y	450.8	0.081	2.73	1.96	0.98	0.68
N120×120×9.0B5II	11.5	1	F	657.8	0.138	1.58	1.14	0.99	2.55
H55×70×4.2B5III	11.4	1	Y	91.6	0.108	1.36	1.31	1.02	0.82
H55×70×4.2B5III-R	11.4	2	Y	109.6	0.137	1.29	1.24	0.93	1.13
H70×55×4.2B5III	15.0	2	Y	72.1	0.128	1.36	1.31	1.06	0.91
H50×95×10.5B5III	2.9	1	F	346.2	0.152	1.68	1.62	0.97	1.13
H95×50×10.5B5III	7.2	1	Y	191.4	0.176	1.57	1.51	0.96	0.85
H64×64×3.0B5III	20.4	3	Y	64.3	0.061	1.20	1.15	0.99	1.00
N70×120×10.5B5III	4.8	1	F	589.7	0.123	2.22	2.14	0.91	1.21
N120×70×10.5B5III	9.6	1	Y	377.7	0.105	2.11	2.04	0.99	1.19
Mean								0.98	
COV								0.061	

^In terms of failure mode, “F” means tensile material fracture and “Y” signifies material yielding and the formation of a plastic collapse mechanism.

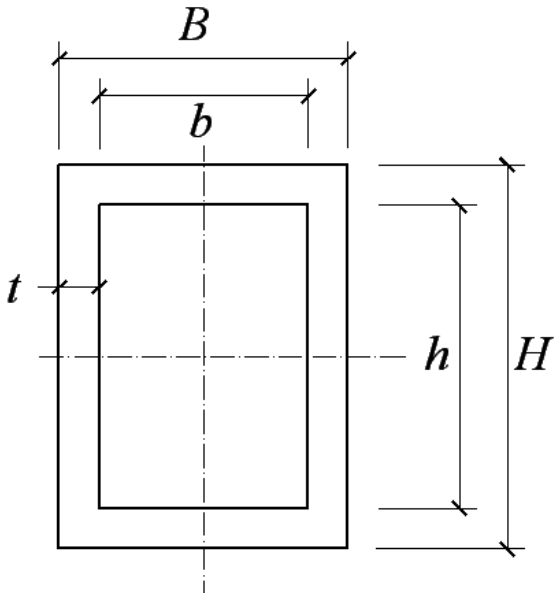

Fig. 1. Definition of symbols for SHS/RHS

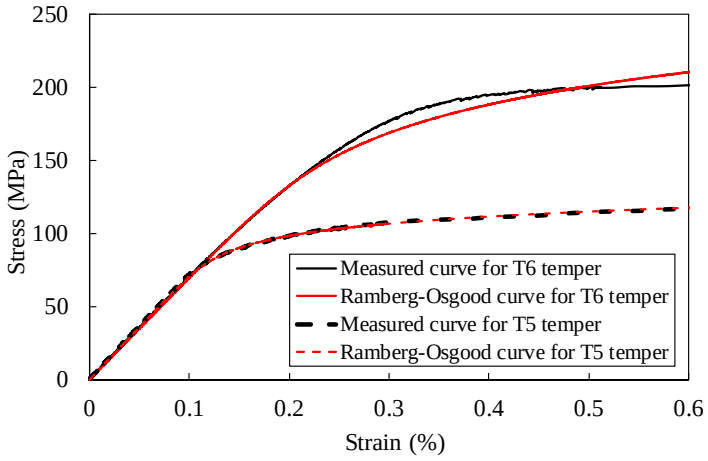

Fig. 2: Typical stress–strain curves of high-strength aluminum alloy 6061-T6 and normal-strength aluminum alloy 6063-T5 measured in this study and predicted from the Ramberg-Osgood model

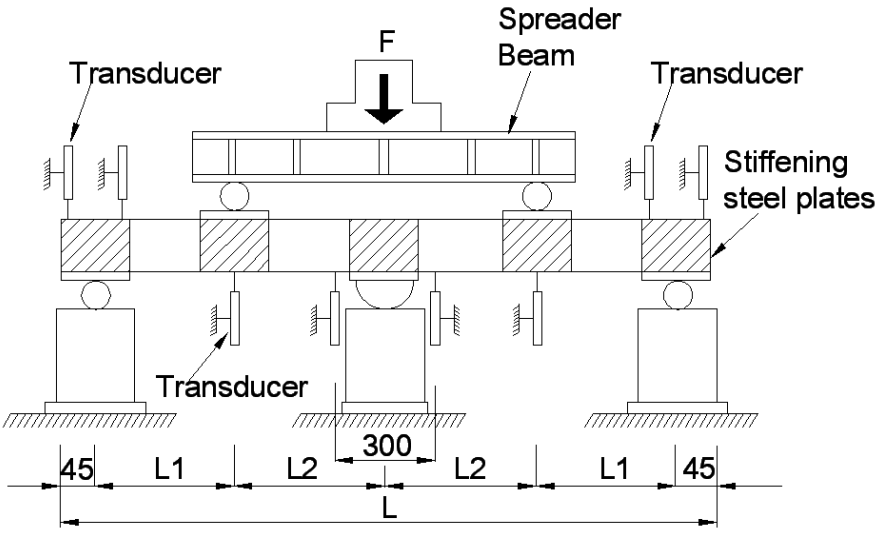

Fig. 3. Schematic illustration of five-point bending configuration (dimensions in mm)

Fig. 4. Experimental setup for five-point bending test

Fig. 5: Deformed five-point bending test specimens (N50×95×10.5B5I, N120×70×10.5B5II and H95×50×10.5B5III)

Fig. 6: Failure of test specimen by material tensile (N70×120×10.5B5III)

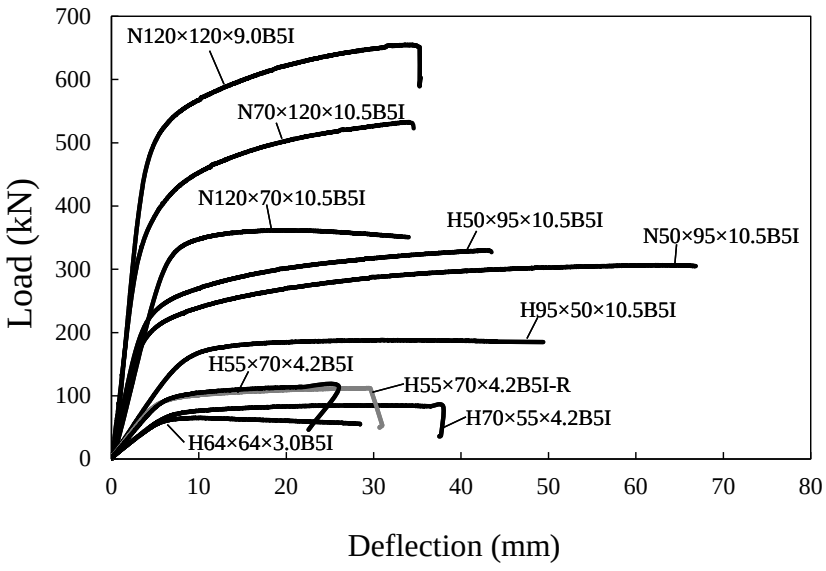

(a)

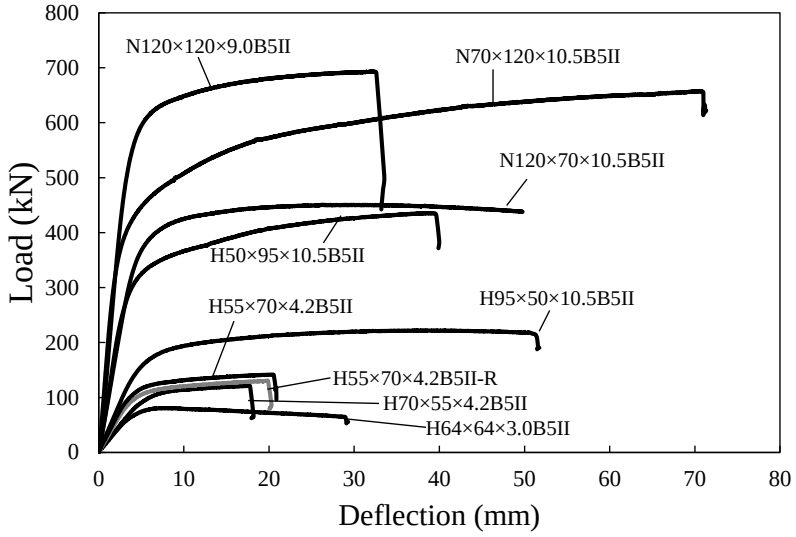

(b)

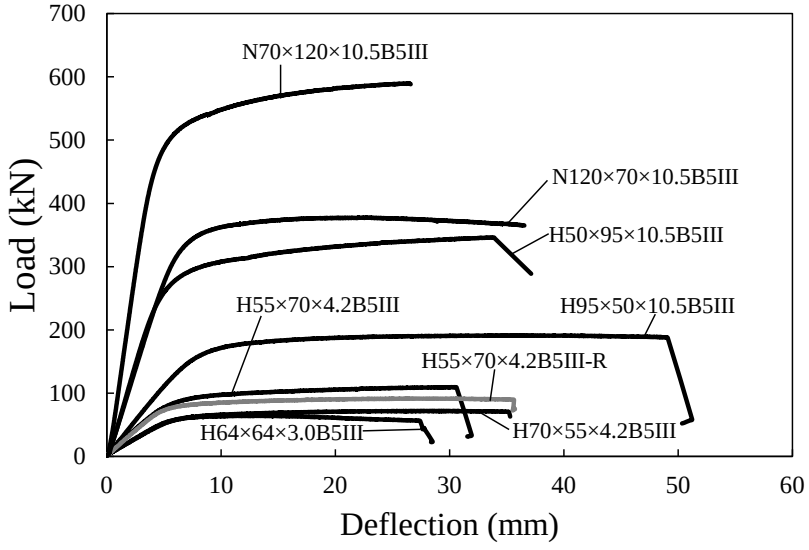

(c)

Fig. 7: Load versus mid-span deflection curves for five-point bending tests of configuration I (a), II (b) and III (c)

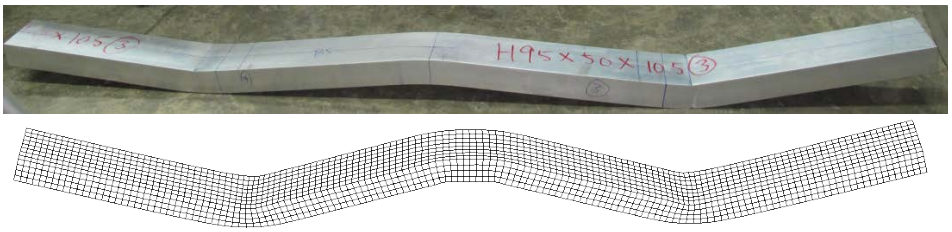

Fig. 8: Experimental and numerical failure modes for specimen H95×50×10.5B5I

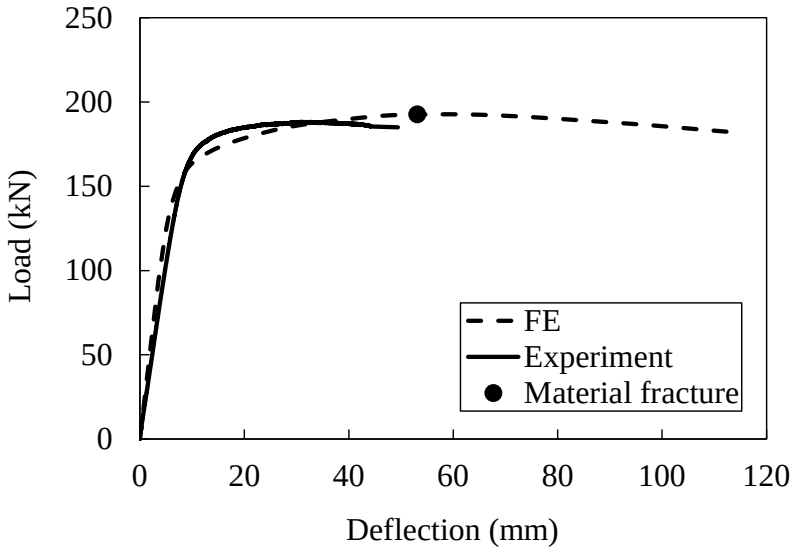

Fig. 9: Experimental and numerical load-deflection curves for specimen H95×50×10.5B5I

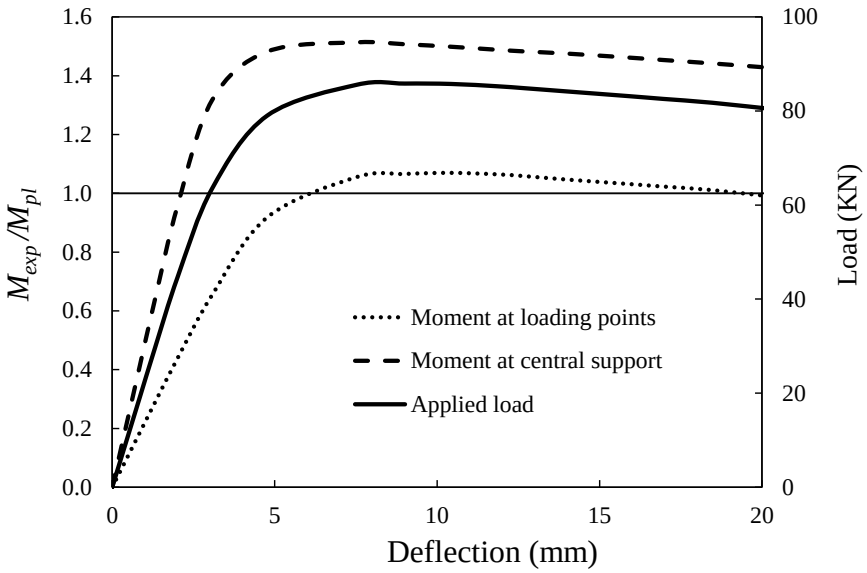

Fig. 10: Applied load and moment displacement curves for specimen H64×64×3.0B5II from finite element models